UNIVERSITAT POLITÈCNICA DE CATALUNYA BARCELONATECH

UPCommons

Portal del coneixement obert de la UPC

http://upcommons.upc.edu/e-prints

Flexible HVDC Transmission Systems Small Signal Modelling: A case study on CIGRE Test MT-HVDC Grid

Seyed Saeid Heidary Yazdi*, Kumars Rouzbehi***, J. Ignacio Candela**
Jafar Milimonfared*, and Pedro Rodriguez**,***
* Amirkabir University of Technology, Tehran, Iran
** Technical University of Catalonia, Barcelona, Spain
***Loyola University Andalucia, Seville, Spain
saedheidary@aut.ac.ir

Abstract—**Future Flexible HVDC Transmission Systems will consist of several active and passive infrastructures including DC Power Flow Controller (DC-PFC) device. The addition of the DC-PFC to the future Multi-Terminal HVDC (MT-HVDC) grids arises some key concerns such as stability, system interoperability, and possible adverse interactions. Hence, a suitable model is necessary to conduct deep frequency domain analysis. In this context, this paper proposes a linearized model for small-signal stability analysis of flexible MT-HVDC grids in state space framework that can be straightforwardly utilized in the process of control design. In this paper, a spick-and-span, systematic and step-by-step process to derive the small signal model of all flexible MT-HVDC grid components is presented such that each sub-system is modeled individually and then all are integrated together. The derived model is cross-verified by time domain simulations of a nonlinear system model in a MATLAB/SIMULINK platform for CIGRE DCS3 MT-HVDC test grid.**

Index Terms—*Cascaded DC power flow controller (CDC-PFC), modular multilevel converter (MMC), multi-terminal HVDC (MT-HVDC) grid.*

I. INTRODUCTION

HVDC based transmission system is a well-accepted solution to exchange cross-border energy, interconnect offshore wind farms to the AC networks and to assist the constitution of the electricity market [1]. Due to the versatility of Voltage Source Converter (VSC)s and recent developments of Modular Multilevel Converter (MMC), erection of Multi-Terminal HVDC (MT-HVDC) systems/grids made possible.

To ensure reliable operation of MT-HVDC systems/grids, several challenges regarding their control and protection should be addressed. In this regard, adequate modeling of MT-HVDC systems is vital. In addition, as the multi-vendor supply of the VSC-HVDCs is expected, future interoperability is a key challenge. Moreover, as the power-flow pattern is passively determined by the MT-HVDC configuration and the resistances seen between the HVDC buses [2] there will be a limited room to adjust the power flow pattern by redacting the set-points of power converters. Therefore, flexible power flow control between the buses is a key factor to enable congestion management, loop flow control, addressing power market requests and avoiding transmission bottlenecks [3]. Possible overloading of a HVDC line can lead to its damage and also a possible cascaded failure of the entire system. Construction of new auxiliary HVDC lines would be a very costly remedy in order to control the line power flow.

The DC-PFC should fulfill requirements regarding its cost, footprint, losses, controllability, and reliability along with fulfillment of its main objective (power flow control) [2], [4, 5]. The objective here is to maximize the exploitation of the existing transmission lines inside their safe and reliable boundaries. Moreover, there are also proposals for utilizing DC-PFCs as HVDC circuit breakers [6], [7]. Lately, the notability of the subject has attracted academia and industry attention. Even CIGRE has motivated to initiate a working group (WG B4-58) devoted to the analysis of the feasibility, methods, and devices for power flow control in MT-HVDC grids [8].

Generally, the DC-PFC devices can be categorized to Cascaded DC-PFC (CDC-PFC) and Serial Parallel DC-PFC (SPDC-PFC) [5]. Benefits such as great controllability and fault blocking capability are entitled to CDC-PFCs [2], [9]. On the other hand, Serial Parallel DC-PFC devices should only withstand a partial (typically around %5) rated system voltage. Therefore, utilization of a full-power converter will be avoided.

The stability and inter-area oscillations in the level of MT-HVDC grids are mainly related to "direct voltage" stability. MT-HVDC grids stability and dynamic performance has been extensively studied in [10]–[[11] and it has been concluded that system stability might be at risk due to instabilities originated by MT-HVDC resonance, weak onshore AC networks, constant power loads and the addition of DC circuit breakers. As a new component is added to the existing MT-HVDC grid, the concerns about system stability, interoperability, possible adverse interactions and highly inductive grid are likely to be increased again. Despite a number of fruitful researches, there is a clear lack of research regarding the in-depth dynamic investigation of the DC-PFC devices and their impacts in MT-HVDC grids.

This research proposes a spick-and-span, systematic and step by step process to derive small signal models of all the flexible MT-HVDC components as subsystems such that each subsystem is modeled individually and then all are interfaced finally. Considering that the origin of possible problems cannot get exhibited by the time domain simulations, hence

frequency domain analysis is required to determine the stability and design suitable remedies and controllers.

The remaining of the paper is structured as follows: dynamic modeling process of the flexible MT-HVDC grid subsystems is derived and presented in section II. Cross-verification of the derived small signal model against nonlinear system model in a MATLAB/SIMULINK platform is presented in Sections III. CIGRE DCS3 test MT-HVDC grid has been considered as the test platform throughout the paper. Finally, key conclusions are drawn in section IV.

II. MODELING OF FLEXIBLE MT-HVDC GRID COMPONENTS

A. Dynamic model of CDC-PFC

An averaged model for the CDC-PFC is shown in Fig.1, neglecting high-frequency switching dynamics as they have a negligible impact on MT-HVDC grid stability. S_m can be used either to enable or bypass the act of power flow control. Also, $n_{c,ff}$ is a feed-forward term obtained from power-flow results and is applied to improve the transient behavior especially in switching between the operation modes. The averaged model consists of two controlled voltage and current sources based on power balance principle as recommendations of [12]. The dependent current source is in parallel with a capacitor (C_p) and a shunt resistance (R_p) connected to the HVDC line. The shunt conductance and capacitance that are presented in the connected HVDC line model are also accumulated with R_p and C_p to facilitate the generalized modeling. In addition, the dependent voltage source is in series with an inductance (L_s) and resistance (R_s) connected to the HVDC bus based on the typical model of DC-DC converters [2]. However, for the static studies (e.g., power-flow) the impacts of inductance and capacitor vanish. Also, here n denotes transformation ratio that is the ratio of the secondary side voltage (v_k) to the primary side voltage (v_i). The CDC-PFC can control the power flowing through the corresponding HVDC line by proper adjustment of the transformation ratio as a control variable.
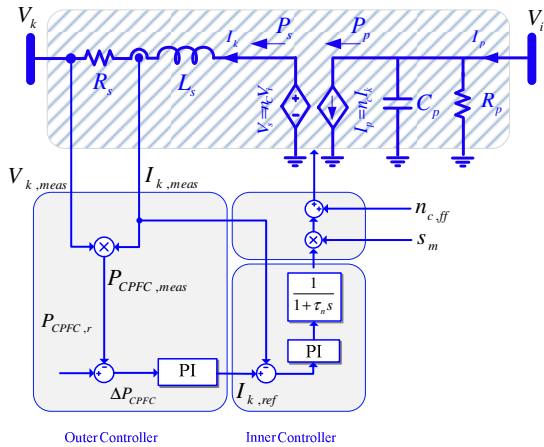

Fig. 1. CDC- PFC averaged model.

The direct current i_k is controlled by an inner current control loop. Also, an outer power control loop is implemented to regulate the flowing power as it is a common command by Transmission System Operator (TSO)s. *However, supplementary control loops might be also implemented to attain certain predefined objectives.* In this study, AC/DC per unit system defined in [13] is adopted. Moreover, a positive power flow direction is considered to be as shown in Fig, 1. The dynamics of direct current can be derived as:

$$\frac{di_k}{dt} = \frac{\omega_b}{L_s}(-R_s i_k - v_k + n v_i) \tag{1}$$

Due to the presence of the term $n v_i$ in (1), the direct current dynamics are nonlinear. This equation can be linearized around the operating point as the following:

$$\frac{d\Delta i_k}{dt} = \frac{\omega_b}{L_s}(-R_s \Delta i_k + n^o \Delta v_i - \Delta v_k + v_i^o \Delta n) \tag{2}$$

In which the superscript "o" and "Δ" refer to the operating point and the deviation from operating point, respectively. As the time is represented in seconds, not in per unit, each derivative term is premultiplied by $1/\omega_b$ factor in the corresponding per-unit equation. It can be eliminated if one also expresses time in per-units and considers $t_b = 1/\omega_b$ as the base value.

The system dynamics associated with the direct voltage (v_i) can be derived and linearized as:

$$\frac{dv_i}{dt} = \frac{\omega_b}{C_p}(-n i_k - \frac{v_i}{R_p} + i_p) \tag{3}$$

$$\frac{d\Delta v_i}{dt} = \frac{\omega_b}{C_p}(-n^o \Delta i_k - \frac{1}{R_p}\Delta v_i - i_{L_s}^o \Delta n + \Delta i_p) \tag{4}$$

For small signal studies, the power flowing through CDC-PFC can be linearized as:

$$\Delta P = i_k^o \Delta v_k + v_k^o \Delta i_k \tag{5}$$

The dynamics of the inner current and outer power control loops are related to the integrator states (x_i and x_p) of the implemented PI controllers ($k_{p2} + k_{i2}/s$ for the power and $k_{p1} + k_{i1}/s$ for the current control loops). Suitable upper and lower output limits are assigned to take the maximum power capacity of CDC-PFC, the maximum current capacity of the HVDC line and permissible range of transformation ratio. Also, clamping based anti wind-up control strategy is applied to avoid undesirable error accumulations (originated from large setpoint changes). Assuming that none of the above-mentioned limitation is violated, the dynamics can be described by:

$$\frac{d\Delta x_p}{dt} = k_{i2}(\Delta P_k^* - \Delta P_k) \tag{5}$$

$$\frac{d\Delta x_i}{dt} = k_{i1}(\Delta i_k^* - \Delta i_k) \tag{7}$$

The bandwidth of the current control loop should be high enough to ensure a fast closed-loop current control response

[14]. However, there is an upper bandwidth bound since it is mandatory for the carrier waveform frequency to be at least 10 times larger than its of modulating waveform in order to warrant high precision for the average model. Also, the bandwidth of the outer power control loop is considered to be significantly (for instance, 10 times) lower than its of the inner current control loop. The reference current (Δi_k^*) and reference transformation ratio (Δn^*) are calculated by outer power and inner current control loops respectively:

$$\Delta i_k^* = k_{p2}(\Delta P^* - \Delta P) + \Delta x_p \tag{8}$$

$$\Delta n^* = k_{p1}(\Delta i_k^* - \Delta i_k) + \Delta x_i \tag{9}$$

It is a common assumption to reflect the control delays (τ_n) originated from the process of the PWM switching and discrete control system by a first order transfer function [15]. Therefore the transformation ratio (Δn) is a state variable and the associated dynamics are:

$$\frac{d\Delta n}{dt} = \frac{1}{\tau_n}(\Delta n^* - \Delta n) \tag{10}$$

Combining (1)–(10) leads to a 4th order model that represent the whole CDC-PFC dynamics. System dynamics can be represented as (11) in which $x = \begin{bmatrix} \Delta i_k & \Delta v_i & \Delta x_p & \Delta x_i & \Delta n \end{bmatrix}^T$ denotes the state variables vector, $w = [\phi]$ is the disturbance vector, $w_l = \begin{bmatrix} \Delta v_k & \Delta i_p \end{bmatrix}^T$ is the linking variables vector that interrelates whole MT-HVDC subsystems together and $u = [\Delta P_k^*]$ is the input vector. Moreover, suitable outputs $y = \begin{bmatrix} i_k & v_i \end{bmatrix}^T$ are defined that plays the role of linking variables into the other subsystems.

$$\frac{dx}{dt} = A_{PFC}x + B_{w,PFC}w + B_{wl,PFC}w_l + B_{u,PFC}u \tag{6}$$

$$y = C_{PFC}x$$

The $A_{PFC}, B_{w,PFC}, B_{wl,PFC}, B_{u,PFC}$ and C_{PFC} are extracted from system dynamics:

$$A_{PFC} = \begin{bmatrix} \dfrac{-\omega_b R_s}{L_s} & \dfrac{\omega_b n^o}{L_s} & 0 & 0 & \dfrac{\omega_b v_i^o}{L_s} \\ -\dfrac{\omega_b n^o}{C_p} & -\dfrac{\omega_b}{R_p C_p} & 0 & 0 & -\dfrac{\omega_b i_k^o}{C_p} \\ -k_{i2}v_k^o & 0 & 0 & 0 & 0 \\ -k_{i1}(k_{p2}v_k^o + 1) & 0 & k_{i1} & 0 & 0 \\ -\dfrac{k_{p1}}{\tau_n}(k_{p2}v_k^o + 1) & 0 & \dfrac{k_{p1}}{\tau_n} & \dfrac{1}{\tau_n} & \dfrac{-1}{\tau_n} \end{bmatrix} \tag{7}$$

$$B_{w,PFC} = [\phi], \quad B_{wl,PFC} = \begin{bmatrix} \dfrac{-\omega_b}{L_s} & 0 \\ 0 & \dfrac{\omega_b}{C_p} \\ -k_{i2}i_k^0 & 0 \\ -k_{i1}k_{p2}i_k^0 & 0 \\ -\dfrac{k_{p1}k_{p2}i_k^0}{\tau_n} & 0 \end{bmatrix} \tag{8}$$

$$B_{u,PFC} = \begin{bmatrix} 0 \\ 0 \\ k_{i2} \\ k_{i1}k_{p2} \\ \dfrac{k_{p1}k_{p2}}{\tau_n} \end{bmatrix}, \quad C_{PFC} = \begin{bmatrix} 1 & 0 & 0 & 0 & 0 \\ 0 & 1 & 0 & 0 & 0 \end{bmatrix} \tag{9}$$

B. Dynamic model of transmission lines

HVDC transmission lines are comprised of Over Head Line (OHL)s and shielded cables. They can be modeled using cascaded π sections approach (Fig. 2) to include an approximation of Electro-Magnetic Transient (EMT) type models in the state space formulation. For studies focused on low-frequency oscillations below 100 Hz, cascaded (say to be n) π sections (and even single lumped) model is sufficiently accurate [11]. However, to analyze intermediate and high-frequency oscillations above 100 Hz, more elaborated frequency dependent models should be considered [16]. Indeed, the generality of modeling approach is preserved. In this way, detailed interpretations about oscillating modes and associated dampings can be drawn. Two capacitor-conductance $C_c - G_p$ and inductor-resistance $L_c - R_c$ branches exist in each π section. Note that the first and last capacitor branch are combined with the model of MMCs and CDC-PFC in order to facilitate the generalized modeling. However, in the presence of HVDC Circuit Breakers (CB)s, line models will be terminated by inductors and such combination will be unnecessary. Also, in the case of intermediate buses [17], the capacitance and conductances of all joining transmission lines are accumulated in order to reduce the number of states and avoid all-*inductor cut-set*.
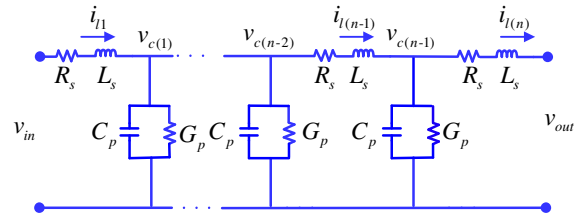

Fig.2. A cascaded π sections model for HVDC line.

The dynamics of MT-HVDC grid lines can be derived considering voltage of the capacitors (v_{c_j}) and current of inductors (i_{l_j}) as the state variables:

$$\frac{dv_{c_j}}{dt}\bigg|_s = \frac{\omega_b}{C_p}(i_{l_j} - i_{l_{j+1}} - G_p v_{c_j}),$$

$$S = \{j \mid j > 0 \text{ and } j < n\} \tag{15}$$

$$\frac{di_{l_j}}{dt}\bigg|_s = \frac{\omega_b}{L_s}(-R_s i_{l_j} + v_{c_{j-1}} - v_{c_j}),$$

$$S = \{j \mid j > 1 \text{ and } j < n\} \tag{16}$$

$$\frac{di_{l_1}}{dt} = \frac{\omega_b}{L_s}(-R_s i_{l_1} - v_{c_1} + v_{in}),$$

$$\frac{di_{l_n}}{dt} = \frac{\omega_b}{L_s}(-R_s i_{l_n} + v_{c_{n-1}} - v_{out}) \tag{17}$$

Combining (15)–(17) leads to a $(2n\text{-}1)^{\text{th}}$ order model that represents the line dynamics in the form of (11). Also, $x = \begin{bmatrix} i_l & | & v_c \end{bmatrix}^T$, $w = [\phi]$, $w_l = \begin{bmatrix} \Delta v_{c_0} & \Delta v_{c_n} \end{bmatrix}^T$ and $u = [\phi]$. Also, the first and last sections inductor current are defined as outputs $y = \begin{bmatrix} i_{l_1} & i_{l_n} \end{bmatrix}^T$ for each line. The whole MT-HVDC grid dynamics can be derived by accumulating the dynamics of constituent lines.

For instance, assuming a lumped model (single π section) for the HVDC lines inside DCS3 (Fig. 2), it is easy to find (18)–(23). For the sake of simplicity, the HVDC buses and lines of the DCS3 are numbered as it is presented in Table I and II. Note that the positive current direction is considered to be as in Table II.

TABLE I.
DCS3 BUS NUMBERS

DC Bus	Bb-A1	Bb-B1	Bb-B2	Bb-B4	Bb-D1
Number	1	2	3	4	5
DC Bus	Bb-C2				
Number	6				

TABLE II.
DCS3 LINE NUMBERS

DC Line	Bb-A1/Bb-B1	Bb-A1/Bb-B4	Bb-B1/ Bb-B4
Number	1	2	3
DC Line	Bb-B4/ Bb-B2	Bb-D1/ Bb-B1	Bb-C2/ Bb-D1
Number	4	5	6
DC Line	Bb-C2/ Bb-A1		
Number	7		

$$x = [\Delta i_{L_1} \quad \Delta i_{L_2} \quad \Delta i_{L_3} \quad \Delta i_{L_4} \quad \Delta i_{L_5} \quad \Delta i_{L_6}$$
$$\Delta i_{L_7} \quad \Delta v_{C_4}]^T \tag{18}$$

$$w_{l,g} = [\Delta v_{dc1} \quad \Delta v_{dc2} \quad \Delta v_{dc3} \quad \Delta v_{dc4} \quad \Delta v_{dc5}]^T \tag{19}$$

$$y = \begin{bmatrix} \Delta i_{L_1} & \Delta i_{L_2} & \Delta i_{L_3} & \Delta i_{L_4} & \Delta i_{L_5} & \Delta i_{L_6} & \Delta i_{L_7} \end{bmatrix} \tag{20}$$

$$A_g = \begin{bmatrix} A_{g1} & A_{g2} \\ A_{g3} & 0 \end{bmatrix}, A_{g1}(i.i) = -\frac{\omega_b R_i}{L_i} \forall i = 1:7,$$

$$A_{g1}(i.j)|_{i \neq j} = 0$$

$$A_{g2} = \begin{bmatrix} 0 & -\frac{\omega_b}{L_2} & -\frac{\omega_b}{L_3} & \frac{\omega_b}{L_4} & 0 & 0 & 0 \end{bmatrix}^T$$

$$A_{g3} = \begin{bmatrix} 0 & \frac{\omega_b}{C_4} & \frac{\omega_b}{C_4} & -\frac{\omega_b}{C_4} & 0 & 0 & 0 \end{bmatrix} \tag{21}$$

$$B_{wl}^{grid} = \begin{bmatrix} \frac{\omega_b}{L_1} & -\frac{\omega_b}{L_1} & 0 & 0 & 0 \\ \frac{\omega_b}{L_2} & 0 & 0 & 0 & 0 \\ 0 & \frac{\omega_b}{L_3} & 0 & 0 & 0 \\ 0 & 0 & -\frac{\omega_b}{L_4} & 0 & 0 \\ 0 & -\frac{\omega_b}{L_5} & 0 & \frac{\omega_b}{L_5} & 0 \\ 0 & 0 & 0 & -\frac{\omega_b}{L_6} & \frac{\omega_b}{L_6} \\ -\frac{\omega_b}{L_7} & 0 & 0 & 0 & \frac{\omega_b}{L_7} \\ 0 & 0 & 0 & 0 & 0 \end{bmatrix}, \tag{22}$$

$$B_w^{grid} = [\phi], \quad B_u^{grid} = [\phi]$$

$$C = \begin{bmatrix} 1 & 0 & 0 & 0 & 0 & 0 & 0 & 0 \\ 0 & 1 & 0 & 0 & 0 & 0 & 0 & 0 \\ 0 & 0 & 1 & 0 & 0 & 0 & 0 & 0 \\ 0 & 0 & 0 & 1 & 0 & 0 & 0 & 0 \\ 0 & 0 & 0 & 0 & 1 & 0 & 0 & 0 \\ 0 & 0 & 0 & 0 & 0 & 1 & 0 & 0 \\ 0 & 0 & 0 & 0 & 0 & 0 & 1 & 0 \end{bmatrix} \tag{23}$$
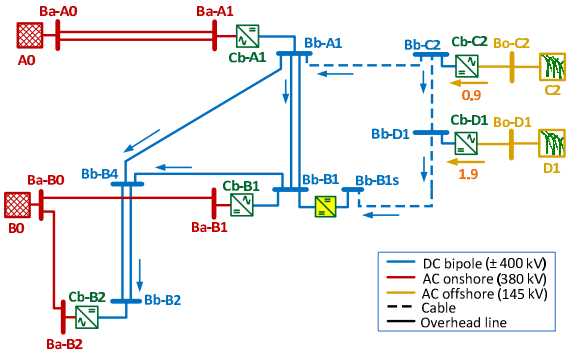

Fig.2. CIGRE DCS3 MT-HVDC grid.

C. Dynamic model of MMC-HVDC

An averaged model for the MMC based VSC-HVDC is shown in Fig. 3 along with its main control loops [18], [19]. Assuming a set of well-balanced Sub-Module (SM) voltages together with the appropriate handling of double frequency circulating current (e.g., by implementing a passive filter or using an extra supplementary control loop [20]), the classical Averaged Value Model (AVM) approach that is widely applied to 2 (and 3)-level converters can be easily generalized to the MMC. The equivalent capacitance can be calculated considering total stored energy in the SMs capacitors, however, the equivalent inductance is calculated by $L_{arm_{dc}} = (2/3)L_{arm}$. Also, R_{loss} which takes conduction losses into account can be extracted from Mitsubishi CM1500HC-66R IGBT module which is implemented in practical projects.
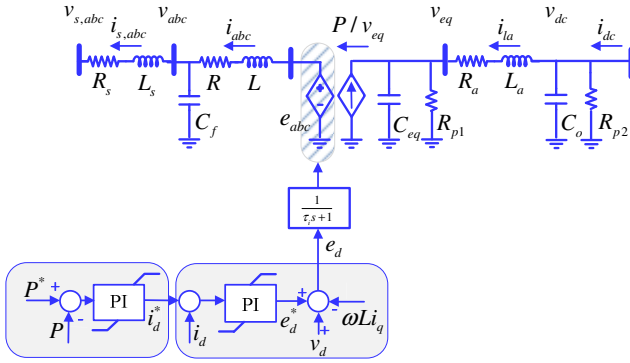

Fig.3. The MMC averaged model and corresponding control system.

The connected grids are assumed not to be very weak (SCR=4) and modeled by an ideal voltage source in series with the Thevinan impedance terminated with filter bus capacitance. A dedicated Phase-Locked Loop (PLL) is utilized to align the direct-axis PCC voltage to the rotating space vector. However, PLL dynamics can be neglected. Also, R and L covers both transformer and arm impedance. Main control loops include inner current control loop with appropriate feed-forward terms to decouple the direct and quadrant axis dynamics, outer power control loop along with the dynamics of PWM and discrete controllers modeled as a first order transfer function [15]. The cautions for controllers bandwidths also hold true here, hence, those corresponding to inner current and outer power control loops are designed to be 200 rad/s and 20 rad/s respectively. The q axis dynamics which have a strong connection to reactive power control are not included since in relatively strong grids the drift of quadrant-axis voltage is well nullified by the synchronization unit and therefore have a negligible impact on d-axis (and power control loops) dynamics. An outer active power output versus direct voltage droop controller might be implemented on some units, however, is not shown in Fig. 3. A 9th order state space model largely adopted from [11] can be derived in the form of (10) with the following state variables, disturbance inputs, linking variable and input vectors:

$$x = [\Delta e_d \quad \Delta v_d \quad \Delta i_d \quad \Delta i_{sd} \quad \Delta x_{id} \quad \Delta x_p \quad (10)$$
$$\Delta v_{eq} \quad \Delta v_{dc} \quad \Delta i_{la}]^T$$

$$w = \begin{bmatrix} \Delta v_{sd} & \Delta v_q & \Delta i_q & \Delta i_{sq} \end{bmatrix}^T, \ w_l = \begin{bmatrix} \Delta i_{dc} \end{bmatrix} \quad (11)$$

$$u = \begin{bmatrix} \Delta P^* \end{bmatrix} \quad (12)$$

The Δx_{id} and Δx_p represents the integrator states of PI controllers adopted in current and power control loops. The A_{c_1}, B_{w,c_1}, B_{wl,c_1}, B_{u,c_1} and C_{c_1} matrices are given in [11] and are not repeated here. It should be noted that there might be VSCs with different power ratings in the grid as DCS3. In this case, the local control of each converter is implemented in per units regarding its own nominal values as base quantities in nonlinear simulations. However, their small signal model is transferred to the univalent per unit system at the final stage to model the whole grid dynamics. It can be done considering that the dimensions of PI controllers in current and power control loops are $[\Omega]$ and $[1/V]$ respectively.

D. Dynamic model of overall flexible MT-HVDC

Having the models of all subsystem in the form of (11) it is easy to derive the whole system state space model by omitting the linking variables by the aid of subsystems outputs. At the first step, the current flowing into MMCs $w_{l,c} = \begin{bmatrix} w_{l,c_1} & w_{l,c_2} & \dots & w_{l,c_n} \end{bmatrix}^T$ and CDC-PFC $\begin{bmatrix} 0 & 1 \end{bmatrix}.w_{l,PFC}$ should be determined based on the grids topology and using MT-HVDC outputs y_g and CDC-PFC (first) output $\begin{bmatrix} 1 & 0 \end{bmatrix} y_{PFC}$. The results are reflected in $\mathbf{I}_{tr}$ and $\mathbf{V}_{tr}$ matrices. Afterwards, the linking variables corresponding to MT-HVDC w_l^g and CDC-PFC (nodal voltages) $\begin{bmatrix} 1 & 0 \end{bmatrix}.w_{l,PFC}$ should be extracted from MMC outputs $y_c = \begin{bmatrix} y_{c_1} & y_{c_2} & \dots & y_{c_n} \end{bmatrix}^T$ along with (second) PFC output $\begin{bmatrix} 0 & 1 \end{bmatrix} y_{PFC}$.

$$w_{l,c} = \begin{bmatrix} \Delta i_{dc_1} \\ \Delta i_{dc_2} \\ \vdots \\ \Delta i_{dc_{n_c}} \end{bmatrix} = \mathbf{I}_{c,g}^{tr} C_g x_g + \mathbf{I}_{c,pfc}^{tr} \begin{bmatrix} 1 & 0 \end{bmatrix} C_{pfc} x_{pfc} \quad (13)$$

$$\begin{bmatrix} 0 & 1 \end{bmatrix} w_{l,PFC} = \mathbf{I}_{tr}^{pfc,g} C_g x_g \quad (14)$$

$$\begin{bmatrix} 1 & 0 \end{bmatrix} w_{l,pfc} = \mathbf{V}_{pfc,c}^{tr} C_c x_c \quad (15)$$

$$w_{l,g} = \mathbf{V}_{g,c}^{tr} C_c x_c + \mathbf{V}_{g,pfc}^{tr} \begin{bmatrix} 0 & 1 \end{bmatrix} C_{pfc} x_{pfc} \quad (16)$$

As a result, the whole MT-HVDC grid dynamics can be represented as below by accumulating MMCs state vectors $x_c = \begin{bmatrix} x_{c_1} & x_{c_2} & \dots & x_{c_n} \end{bmatrix}^T$, disturbance inputs $w_c = \begin{bmatrix} w_{c_1} & w_{c_2} & \dots & w_{c_n} \end{bmatrix}^T$ and inputs $u_c = \begin{bmatrix} u_{c_1} & u_{c_2} & \dots & u_{c_n} \end{bmatrix}^T$.

$$\frac{d}{dt}\begin{bmatrix} x_c \\ x_{pfc} \\ x_g \end{bmatrix} = A_{F-MT-HVDC}\begin{bmatrix} x_c \\ x_{pfc} \\ x_g \end{bmatrix} + \begin{bmatrix} B_{w,c} & \mathbf{0} & \mathbf{0} \\ \mathbf{0} & \mathbf{0} & \mathbf{0} \\ \mathbf{0} & \mathbf{0} & \mathbf{0} \end{bmatrix}\begin{bmatrix} w_c \\ w_{pfc} \\ w_g \end{bmatrix}$$

$$+ \begin{bmatrix} B_{u,c} & \mathbf{0} & \mathbf{0} \\ \mathbf{0} & B_{u,pfc} & \mathbf{0} \\ \mathbf{0} & \mathbf{0} & \mathbf{0} \end{bmatrix} \tag{31}$$

$$A_{F-MT-HVDC} =$$

$$\begin{bmatrix} A_c & B_{w_l,c}\mathbf{I}^{tr}_{c,pfc}[1 \quad 0]C_{pfc} & B_{w_l,c}\mathbf{I}^{tr}_{c,g}C_g \\ B_{w_l,c}\begin{bmatrix}1\\0\end{bmatrix}\mathbf{V}^{tr}_{pfc,c}C_c x_c & A_{pfc} & B_{w_l,pfc}\begin{bmatrix}0\\1\end{bmatrix}\mathbf{I}^{tr}_{pfc,g}C_g \\ B_{w_l,g}\mathbf{V}^{tr}_{g,c}C_c & B_{w_l,g}\mathbf{V}^{tr}_{g,pfc}[0 \quad 1]C_{pfc} & A_g \end{bmatrix}$$

$$B_{w,c} = diag(B_{w,c_1} \quad B_{w,c_2} \quad \cdots \quad B_{w,c_n}),$$

$$B_{u,c} = diag(B_{u,c_1} \quad B_{u,c_2} \quad \cdots \quad B_{u,c_n}), \tag{32}$$

$$C_c = diag(C_{c_1} \quad C_{c_2} \quad \cdots \quad C_{c_n})$$

III. CROSS VERIFICATION OF THE LINEARIZED MODEL

To have a reference model in order to verify the small signal model, the DCS3 grid detailed nonlinear model is simulated in a MATLAB/SIMULINK platform. The parameters stated in [12] are used as the starting point. Converters control system is implemented in per units and in rotating reference frame with the d-axis voltage aligned to the PCC voltage space vector. Active power output versus direct voltage droop controllers are applied to all power converters except Cb-D1 and Cb-C2 that mimics the behavior of an offshore wind farm and normally do not participate in the MT-HVDC grid voltage control.

To verify the authenticity of the linearized model, the simulation results corresponding to the nonlinear model are compared to those of linearized model.

Figures 4.(a) to 4.(c) show the system response to a -29.511% CDC-PFC power set point change (from 0.29511 pu to 0 pu) on main system states (MMCs output voltages $[v_{dc1} \quad v_{dc2} \quad \cdots \quad v_{dc5}]^T$ and CDC-PFC output current i_k). The dashed and solid lines delegate the responses of linear and nonlinear model respectively and the bus numbers are according to Table .1.

The sudden current nulling at the line between buses Bb-D1 to Bb-B1, in which the CDC-PFC is present there, results in direct voltage oscillations inside the MT-HVDC grid. However, the most severe excursions are visible in the bus voltages 2 and 4 at the very beginning of the transient. It is evident that the key states are accurately estimated by the linearized model in terms of overall behavior, settling times, time constants and over (under) shoot values. There is a small deviation in deviating from the operating point that is mainly due to the nonlinearity present in the power equation of MMCs and CDC-PFC. However, it is negligible unless in significant excursions from the linearized point. Hence, the validity of the model is proved.
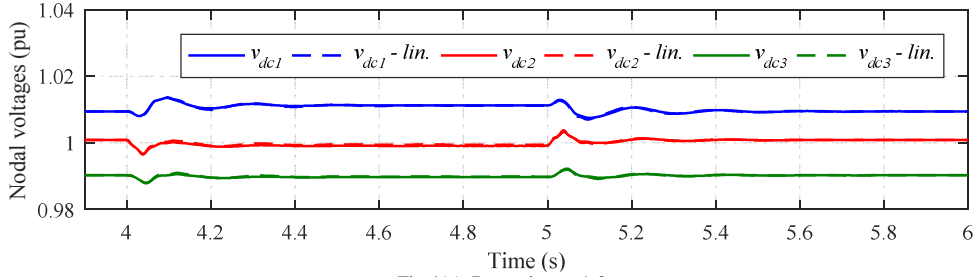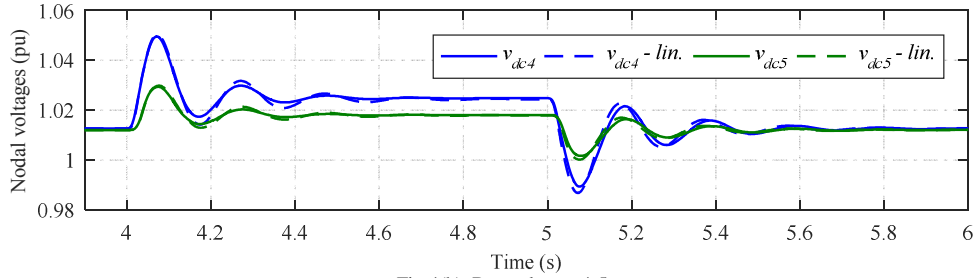

Fig.4(a). Bus voltages 1-3.
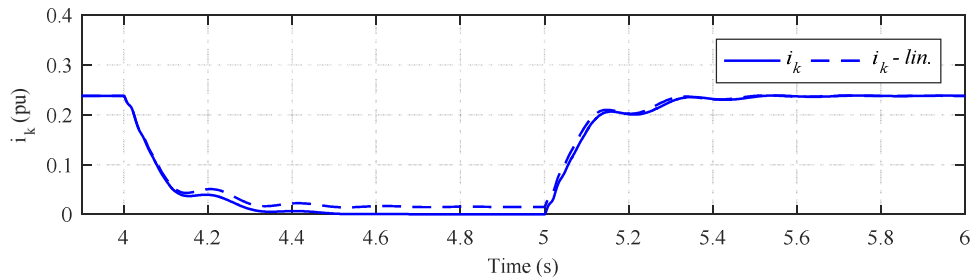

Fig.4(b). Bus voltages 4-5.

Fig.4(c). The CDC-PFC current.

IV. CONCLUSION

Several DC Power Flow Controller (DC-PFC)s are proposed and integrated to the understudy Multi-Terminal HVDC (MT-HVDC) grids in last years. These emerging devices pose a major concern when it comes to systems stability, interoperability, and possible adverse interactions. In this regard, identification of suitable small-signal model for DC-PFC is a cardinal task to analyze their contribution to system dynamics which was the subject of this paper. A 4th order model is derived for the cascaded DC-PFC that includes the DC-DC converter, outer power control loop, inner current control loop and the effect of the delays originated from the act of PWM and discrete controllers. A systematic and step by step small signal modeling approach is derived accordingly and its credibility is evaluated considering CIGRE DCS3 test grid. Simulation results in MATLAB/SIMULINK revealed that the obtained model is indeed accurate for analyzing the future flexible MT-HVDC dynamics and is authentic for future studies regarding control design.

REFERENCES

[1] P. RODRIGUEZ and K. ROUZBEHI, "Multi-terminal DC grids: challenges and prospects," *Journal of Modern Power Systems and Clean Energy,* vol. 5, pp. 515-523, July 01 2017.

[2] K. Rouzbehi, J. I. Candela, A. Luna, G. B. Gharehpetian, and P. Rodriguez, "Flexible Control of Power Flow in Multiterminal DC Grids Using DC-DC Converter," *IEEE Journal of Emerging and Selected Topics in Power Electronics,* vol. 4, pp. 1135-1144, 2016.

[3] J. Sau-Bassols, E. Prieto-Araujo, and O. Gomis-Bellmunt, "Modelling and Control of an Interline Current Flow Controller for Meshed HVDC Grids," *IEEE Transactions on Power Delivery,* vol. 32, pp. 11-22, 2017.

[4] K. Rouzbehi, A. Miranian, J. I. Candela, A. Luna, and P. Rodriguez, "A hybrid power flow controller for flexible operation of multi-terminal DC grids," in *2014 International Conference on Renewable Energy Research and Application (ICRERA)*, 2014, pp. 550-555.

[5] K. Rouzbehi, A. Miranian, J. I. Candela, A. Luna, and P. Rodriguez, "Proposals for flexible operation of multi-terminal DC grids: Introducing flexible DC transmission system (FDCTS)," in *2014 International Conference on Renewable Energy Research and Application (ICRERA)*, 2014, pp. 180-184.

[6] M. J. Carrizosa, J. Cortés, A. Benchaib, P. Alou, G. Damm, J. A. Cobos*, et al.*, "DC / DC converters as DC circuit-breakers in HVDC networks operation," in *2014 16th European Conference on Power Electronics and Applications*, 2014, pp. 1-10.

[7] M. Hajian, D. Jovcic, and B. Wu, "Evaluation of Semiconductor Based Methods for Fault Isolation on High Voltage DC Grids," *IEEE Transactions on Smart Grid,* vol. 4, pp. 1171-1179, 2013.

[8] C. W. B4-58. (2016). *Devices for Load flow Control and Methodologies for Direct Voltage Control in a Meshed HVDC Grid.* Available: http://b4.cigre.org/

[9] T. Lüth, M. M. C. Merlin, T. C. Green, F. Hassan, and C. D. Barker, "High-Frequency Operation of a DC/AC/DC System for HVDC Applications," *IEEE Transactions on Power Electronics,* vol. 29, pp. 4107-4115, 2014.

[10] G. Pinares and M. Bongiorno, "Analysis and Mitigation of Instabilities Originated From DC-Side Resonances in VSC-HVDC Systems," *IEEE Transactions on Industry Applications,* vol. 52, pp. 2807-2815, 2016.

[11] W. Wang, M. Barnes, O. Marjanovic, and O. Cwikowski, "Impact of DC Breaker Systems on Multiterminal VSC-HVDC Stability," *IEEE Transactions on Power Delivery,* vol. 31, pp. 769-779, 2016.

[12] T. K. Vrana, Y. Yang, D. Jovcic, S. Dennetière, J. Jardini, and H. Saad, "The CIGRE B4 DC Grid Test System," 2016.

[13] A. Yazdani and R. Iravani, *Voltage-Sourced Converters in Power Systems:Modeling, Control, and Applications*: Wiley-IEEE Press 2010.

[14] K. Rouzbehi, A. Miranian, A. Luna, and P. Rodriguez, "Optimized Control of Multi-Terminal DC Grids Using Particle Swarm Optimization," *EPE Journal,* vol. 24, pp. 38-49, 2014/06/01 2014.

[15] B. Bahrani, S. Kenzelmann, and A. Rufer, "Multivariable-PI-Based dq Current Control of Voltage Source Converters With Superior Axis Decoupling Capability," *IEEE Transactions on Industrial Electronics,* vol. 58, pp. 3016-3026, 2011.

[16] J. Beerten, S. D. Arco, and J. A. Suul, "Frequency-dependent cable modelling for small-signal stability analysis of VSC-HVDC systems," *IET Generation, Transmission & Distribution,* vol. 10, pp. 1370-1381, 2016.

[17] E. Prieto-Araujo, F. D. Bianchi, A. Junyent-Ferre, and O. Gomis-Bellmunt, "Methodology for Droop Control Dynamic Analysis of Multiterminal VSC-HVDC Grids for Offshore Wind Farms," *IEEE Transactions on Power Delivery,* vol. 26, pp. 2476-2485, 2011.

[18] H. Saad, J. Peralta, S. Dennetière, J. Mahseredjian, J. Jatskevich, J. A. Martinez*, et al.*, "Dynamic Averaged and Simplified Models for MMC-Based HVDC Transmission Systems," *IEEE Transactions on Power Delivery,* vol. 28, pp. 1723-1730, 2013.

[19] H. Saad, S. Dennetière, J. Mahseredjian, P. Delarue, X. Guillaud, J. Peralta*, et al.*, "Modular Multilevel Converter Models for Electromagnetic Transients," *IEEE Transactions on Power Delivery,* vol. 29, pp. 1481-1489, 2014.

[20] Q. Tu, Z. Xu, and L. Xu, "Reduced Switching-Frequency Modulation and Circulating Current Suppression for Modular Multilevel Converters," *IEEE Transactions on Power Delivery,* vol. 26, pp. 2009-2017, 2011.